Estimating the impact of school closures on COVID-19 disease burden

Supplementary Appendix

——— Add Authors List here ———

Contents

1 Model description

1.1 General approach

We use a semi-mechanistic compartmental model of COVID-19 transmission governed by ordinary differential equations (ODEs). Our model captures important factors of COVID-19 transmission and disease such as age-specific characteristics, heterogeneous mixing, vaccination and the emergence of different variants of concern. The ODE-based model is used to capture only states relevant to transmission, whereas hospitalisations and deaths are estimated through a convolution process applied to the ODE-based model's outputs. This process combines the model-estimated disease incidence with statistical distributions modelling the time to hospitalisation, the hospital stay duration and the time to death. This approach presents two main advantages. First it reduces the complexity of the dynamic system relying on numerical solving of ODEs, which is computationally expensive. Second, the convolution approach allows for more flexibility and produces more realistic assumptions regarding the timings of hospitalisations and deaths, compared to what could be achieved with a simple compartmental approach. The following sections describe the model in details and Figure S1 summarises the overall approach used in our analysis.

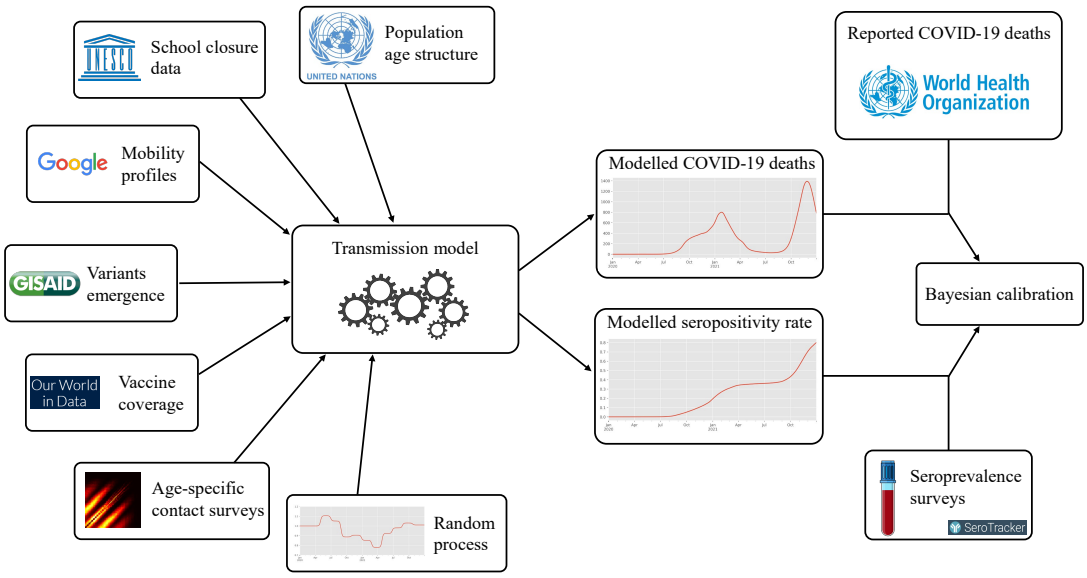

Figure S1: Conceptual approach used to build and calibrate the models

1.2 Transmission model

1.2.1 Compartment types and sequence

Model compartments represent sequential progressions through the processes of infection with, progression through, and recovery from the phases of SARS-CoV-2 infection and COVID-19 disease. The following types of compartments are implemented:

- Susceptible
  - Persons not previously infected with SARS-CoV-2 during or before the model simulation period
- Latent
  - Persons recently infected with SARS-CoV-2, but not in the active phase of the disease yet.
  - These individuals may still be infectious (see details in next paragraph).
- Active

  - Persons with active COVID-19 who are currently infectious.

- Recovered
  - Persons recovered from COVID-19 during the model simulation period
  - Reinfection from these compartments is permitted through exposure to a different strain than the one that most recently infected the individual (see strain stratification section for details).

The base model structure consists of a sequence of one susceptible compartment (S), four latent compartments (E_1, ..., E_4), four active disease compartments (I^1, ..., I^4) and one recovered compartment (R) (Figure S2).

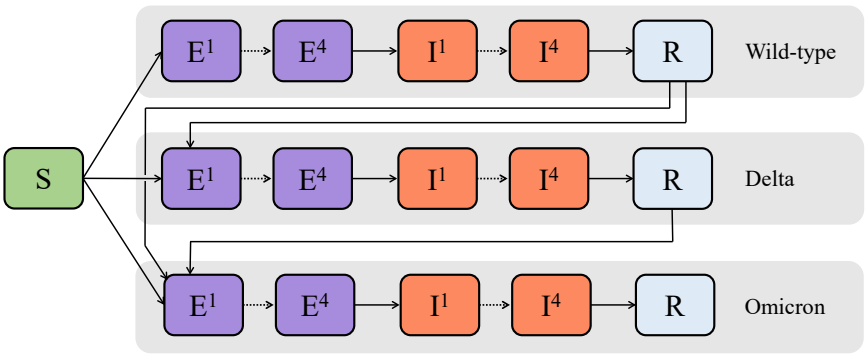

Figure S2: Compartmental model structure. S = Susceptible, E = Exposed / Latent, I = Active disease, R = Recovered. Stratification by age and vaccination status are not shown here.

The main rationale for using four serial compartments for both the latent and active states is to achieve an Erlang distribution for the time spent in each of these states. This distribution is more realistic than the exponential distribution which is the consequence of a single compartment assumption, because the Erlang distribution does not have a large density mass around 0 and is not heavy-tailed. Figure S3 illustrates the modelled distributions of the incubation period and the active disease period.

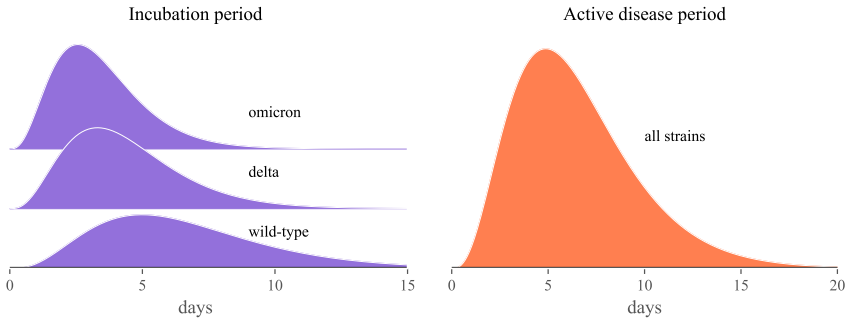

Figure S3: Modelled distributions of the incubation and active disease periods. Active disease period shown for an average duration of 8 days, but this parameter is varied during calibration.

The four active disease compartments all have identical characteristics. However, the last two latent compartments (E^3 and E^4) are infectious whereas the first two (E^1 and E^2) are not. We further assume that the infectious latent compartments are half as infectious as the active disease compartments.

1.2.2 Model stratification by age

All compartments of the base compartmental structure were stratified by age into the following age bands: zero to 14 years / 15 to 24 years / 25 to 49 years / 50 to 69 years / 70 years and above.

The initial population was distributed between the different age bands to reflect the age distributions reported by the United Nations Population Division. Demographic processes, including births, ageing and non-infection-related deaths are not simulated, given the timeframes considered in this simulation.

We assumed heterogeneous mixing between the different age groups to account for the assortative nature of social interactions by age (see Section 1.2.5). Age was assumed to affect:

- The susceptibility to infection
- The risk of COVID-19 hospitalisation
- The risk of COVID-19 death
- The vaccination rate (see Section 1.2.3)

1.2.3 Capturing the effects of vaccination

History of vaccination was captured by stratifying all model compartments by vaccination status. Two vaccination strata were included to represent those who have received at least two doses of a COVID-19 vaccine, and those who have not.

We used data from *Our World in Data* to inform the modelled dynamic vaccination coverage. In particular, we used the reported proportion of people "fully vaccinated" to specify the time-variant proportion of vaccinated people in our model. We assumed that older individuals are vaccinated first by prioritising the modelled age groups in descending order. That is, the oldest age group receives all available vaccines until a saturation coverage of 80% is reached for this group. Then the next oldest category starts receiving vaccines and we repeat this process until all available vaccines are allocated. Note that in the event that the population-level vaccine coverage exceeds 80%, the saturation coverage was set equal to the population-level coverage.

Let us consider two successive time points t_i and t_{i+1} for which vaccination data are available. Let us denote $r_{a,i}$ and $r_{a,i+1}$ the associated vaccine coverage for age group a. The time-variant and age-specific vaccination rate per capita $w_a(t)$ verifies:

$$1 - r_{a,i+1} = (1 - r_{a,i})e^{-w_a(t)(t_{i+1}-t_i)} \quad ,\forall t \in [t_i, t_{i+1}). \tag{1}$$

Then,

$$w_a(t) = \frac{\ln(1 - r_{a,i}) - \ln(1 - r_{a,i+1})}{t_{i+1} - t_i} \quad ,\forall t \in [t_i, t_{i+1}), \tag{2}$$

where $\ln(x)$ represents the natural logarithm of x.

Figure S4 shows the modelled vaccination coverage over time against the reported data for the analysed countries.

The effect of vaccination on transmission is to reduce the rate of infection partially for all persons at-risk of infection in the vaccinated stratum. This includes both fully susceptible (never previously infected) persons, as well as recovered persons who are at risk of reinfection. The model allows for hybrid immunity in the sense that the vaccination-induced relative reduction of transmission risk is multiplied with that induced by previous infection. Vaccination is also assumed to reduce the risk of hospitalisation and death

Emerging variants of concern (VoCs) may partially escape vaccine-induced (as well as infection-induced) immunity, as described further below (Table S2 and Section 1.2.4).

1.2.4 Modelling multiple viral strains

The model was stratified by "strain" to simulate the emergence of multiple variants of concern (VoC). This approach explicitly represents multiple competing strains, each with an independent force of infection calculation. We assumed that VoCs can have different levels of transmissibility, incubation period and disease severity (hospitalisation and death risks) compared to the ancestral COVID-19 strain. In addition, VoCs were assumed to escape immunity partially for both vaccination- and infection-related immunity.

We assumed that individuals previously infected with the wild-type strain could only be reinfected with the delta or omicron strains. However, such individuals have a reduced risk of infection with these variants compared to infection-naive individuals (82% and 45% reduction for delta and omicron,

respectively) [22]. We assumed that individuals previously infected with the delta variant could only be reinfected with the omicron variant, with an infection risk reduced by 45% compared to infection-naive individuals [22]. The other parameters used to represent strain-specific characteristics are presented in Table S2.

Seeding of each new strain into the model was achieved through the importation of a small number (10 per million population) of new infectious persons with the relevant strain into the model. The seeding process was done over a ten-day period and the start of this period was set to the emergence date reported by GISAID for each country [5].

1.2.5 Dynamic social mixing

The model captures changes in social interactions over time through a dynamic age-specific mixing matrix. The following sections describe how this matrix was defined and how it captures the different non-pharmaceutical interventions implemented in the analysed countries, including school closures. The overall approach is also illustrated by Figure S6.

1.2.5.1 Reference mixing matrices

We extracted country-specific contact matrices using the *conmat* R package which derives social mixing matrices from contact survey data. These matrices provide the average numbers of contacts per day between different age groups, disaggregated by the following locations: home, school, work, other locations.

The overall contact matrix (before adjustments for mobility changes) results from the summation of the four location-specific contact matrices: $C_0 = C_H + m_S C_S + C_W + C_L$, where C_H, C_S, C_W and C_L are the age-specific contact matrices associated with households, schools, workplaces and other locations, respectively. Note that the school contribution C_S is multiplied by the factor m_S that was varied during model calibration (see Section 3), in order to account for uncertainty around the relative contribution of school contacts to overall mixing.

1.2.5.2 Modifications of contact rates over time

To capture mobility changes over time, the contributions of the matrices C_S, C_W and C_L vary with time such that the input contact matrix can be written as:

$$C(t) = h(t)^2 C_H + s(t)^2 m_S C_S + w(t)^2 C_W + l(t)^2 C_L \tag{3}$$

The modifying functions h (for households), s (for schools), w (for work) and l (for other-locations) were each squared to capture the effect of the mobility changes on both the infector and the infectee in any given interaction that could potentially result in transmission.

School closure/re-opening

Reduced attendance at schools was represented through the function s, which represents the proportion of all school students currently attending on-site teaching. If schools are fully closed at time t, $s(t) = 0$ and C_S does not contribute to the overall mixing matrix $C(t)$. The function s was derived from the UNESCO database on school closures from the start of the COVID-19 pandemic [23]. This database provides school opening status over time as a categorical variable taking the following values: "Fully open", "Partially open", "Academic break", "Closed due to COVID-19". Table S1 indicates how the different categorical values were converted into the numerical function s.

Table S1: Assumed percentage of students on-site for the different UNESCO school closure categories.

UNESCO category	**Assumed proportion of students on-site at national level ($s(t)$)**
Fully open	100%
Partially open	10-50%
Academic break	0%
Closed due to COVID-19	0%

We included uncertainty around the value associated with the partial closure category, as there was no quantitative data available to inform this parameter [23]. The partial closure periods are likely to be periods where only a small fraction of students such as children of "essential workers" were attending school. We assumed that between 10 and 30% of students attended on-site learning during these periods.

To model the counterfactual "no school closure" scenario, we assumed that the schools were "Fully open" during the periods reported as "Partially open" or "Closed due to COVID-19".

Figure S5 summarises the UNESCO data on school closure for the analysed countries.

Dynamic mobility outside of schools and homes

Changes to people's mobility in places other than schools and homes were modelled using Google Mobility data, after applying a seven-day moving average smoothing. We used the "Workplace" category of the Google data to scale the work-related matrix contribution C_W to overall mixing over time, using the adjusting function w. The "other locations" matrix C_L was scaled through the adjusting function l which was defined as the average of the Google mobility indicators across the following Google categories: "Retail and recreation", "Grocery and pharmacy" and "Transit stations".

Household contacts

In the base case analysis, the contribution of household contacts to the overall mixing matrix was fixed over time (i.e. $h(t) = 1$ in Equation 3). Although Google provides mobility estimates for residential contacts, the nature of these data is different from that of each of the other Google mobility types. They represent the time spent in that location, as opposed to other categories, which measure a change in total visits rather than the duration. The daily frequency with which people attend their residence is likely to be close to one, and we considered that household members likely have a daily opportunity for infection with each other household member regardless of the background level of mobility. Therefore, we did not implement a function to scale the contribution of household contacts to the mixing matrix with time.

1.2.5.3 Sensitivity analyses around dynamic social mixing

In addition to the Base Case analysis described above, we performed two sensitivity analyses considering different assumptions for the modelled social mixing.

SA1: No Google mobility data In a first sensitivity analysis (SA1), we removed the contribution of the Google mobility data to the modelled social mixing (see Figure S6). In this configuration, the calibrated random process ($W(t)$) was used to capture mobility changes implicitly.

SA2: School closures increase household contact rates In another sensitivity analysis (SA2), we considered an alternative assumption under which the effective contact rates within households were increased during periods of school closure. In that case, the household component of the mixing matrix is modified by the following function:

$$h(t) = 1 + 0.20(1 - s(t)) \quad ,$$

where s is the function modifying school contacts as introduced in Section 1.2.5.2. This is equivalent to assuming that each individual has 20% more household contact potential when schools are fully closed.

1.2.6 Random transmission adjustment

The risk of SARS-CoV-2 transmission per contact was adjusted by a time-variant random process, making the model semi-mechanistic. This random process reflects the fact that all the variations observed in the transmission risk in the real world cannot be explained solely by the factors that are explicitly captured through model inputs such as vaccination, dynamic mobility or new variants' emergence. We therefore allowed for random perturbations to the risk of transmission over time, although these perturbations were highly auto-correlated to avoid unrealistic changes over a short period of time.

We used a random walk with Gaussian update defined by:

$$\begin{aligned} W(0) &= 0 \\ W(t+1) &\sim \mathcal{N}(W(t), 0.5) \quad , \end{aligned} \tag{4}$$

where $\mathcal{N}$ denotes the normal distribution. The random process W was updated every two months and was transformed using the exponential function before being applied to the risk of transmission per

contact (see Equation 6). Finally, the contribution of the random process to the risk of transmission was squared in order to capture its effect on both the susceptible and the infectious individuals (see Equation 6).

1.2.7 Ordinary differential equations

Let us first introduce some new notations. Modelled age groups are indicated by the subscript a, and $\mathcal{A}$ represents the set of all modelled age groups (see Section 1.2.2). Vaccination status is represented by the subscript v, and $\mathcal{V}$ is the set of vaccination statuses (i.e. $\mathcal{V} = \{\text{“0”, “1”}\}$, where “0” represents unvaccinated people and “1” represents vaccinated people). The subscript s is used to represent the different viral strains, and $\mathcal{S}$ is the set of all strains (i.e. $\mathcal{S} = \{\text{“wild-type”, “delta”, “omicron”}\}$). The average incubation period duration associated with strain s is denoted q_s and the average duration of active disease is denoted w. The relative susceptibility to infection with strain s of individuals aged a with vaccination status v is denoted $\rho_{a,v,s}$. The term $b_{a,v,s}(t)$ designates the introduction of individuals of age a and with vaccination status v that are infected with strain s (infection seeding). Vaccination is characterised by the age-specific and time-variant per-capita vaccination rate w_a. Finally, $\chi_{s,\sigma}$ represents the relative susceptibility to infection with strain σ for individuals whose most recent infection episode was with strain s. Using this new notation combined with those previously introduced, we can describe the model with the following set of ordinary differential equations:

$$
\begin{aligned}
\frac{dS_{a,v}}{dt} &= -\sum_{s\in\mathcal{S}} \lambda_{a,s}(t)\rho_{a,v,s}S_{a,v} + \Phi_v\omega_a(t)S_{a,v=0} \quad , \\
\frac{dE^1_{a,v,s}}{dt} &= \lambda_{a,s}(t)\rho_{a,v,s}\Big(S_{a,v} + \sum_{\sigma\in\mathcal{S}} \chi_{\sigma,s}R_{a,v,\sigma}\Big) - \frac{4}{q_s}E^1_{a,v,s} + \Phi_v\omega_a(t)E^1_{a,v=0,s} \quad , \\
\frac{dE^k_{a,v,s}}{dt} &= \frac{4}{q_s}E^{k-1}_{a,v,s} - \frac{4}{q_s}E^k_{a,v,s} + \Phi_v\omega_a(t)E^k_{a,v=0,s} \quad , \forall k \in \{2,3,4\}, \\
\frac{dI^1_{a,v,s}}{dt} &= \frac{4}{q_s}E^4_{a,v,s} - \frac{4}{w}I^1_{a,v,s} + b_{a,v,s}(t) + \Phi_v\omega_a(t)I^1_{a,v=0,s} \quad , \\
\frac{dI^k_{a,v,s}}{dt} &= \frac{4}{w}I^{k-1}_{a,v,s} - \frac{4}{w}I^k_{a,v,s} + \Phi_v\omega_a(t)I^k_{a,v=0,s} \quad , \forall k \in \{2,3,4\}, \\
\frac{dR_{a,v,s}}{dt} &= \frac{4}{w}I^4_{a,v,s} - \sum_{\sigma\in\mathcal{S}} \lambda_{a,\sigma}(t)\rho_{a,v,\sigma}\chi_{s,\sigma}R_{a,v,s} + \Phi_v\omega_a(t)R_{a,v=0,s} \quad ,
\end{aligned}
\tag{5}
$$

where $\lambda_{a,s}$ represents the force of infection of strain s affecting individuals of age a. The quantity Φ_v is a binary variable used to switch between a positive and negative multiplier depending on vaccination status. It is equal to 1 when $v =$“1” and -1 when $v =$“0”. In other words, $\Phi_v = 2\mathbb{1}_{v=\text{“1”}} - 1$.

The force of infection was calculated as:

$$
\lambda_{a,s}(t) = \beta e^{2W(t)}\psi_s \sum_{\alpha\in\mathcal{A}}\sum_{v\in\mathcal{V}} \frac{c_{a,\alpha}(t)}{N_{\alpha,v}}\Big(0.5\sum_{k=3}^{4} E^k_{\alpha,v,s} + \sum_{k=1}^{4} I^k_{\alpha,v,s}\Big) \quad . \tag{6}
$$

In the previous equation, β represents the unadjusted risk of transmission per contact, ψ_s is the relative infectiousness of strain s, and $W(t)$ is the random process introduced in Section 1.2.6. The size of the population of age α with vaccination status v is denoted $N_{\alpha,v}$. The term $c_{a,\alpha}(t)$ is a single element of the contact matrix $C(t)$ introduced in Equation 3. It represents the average numbers of contacts per day that a individual of age a has with individuals of age α.

1.2.8 Model parameters

The model parameters and their values (or associated prior distributions) are listed in Table S2.

1.3 Estimation of COVID-19-related hospital pressure and deaths

The transmission model described in Section 1.2 provides estimates of COVID-19 incidence over time, disaggregated by age, vaccination status and strain. We combine these incidence estimates with the age-,

Table S2: Model parameters

Parameter	Value/Distribution	Evidence
Transmission probability per contact [C]	Uniform (0.01, 0.06)	Calibrated
Mean active disease period (days)	6.5	[21, 7, 12]
Country-specific IFR multiplier (m_C) [C]	Uniform (0.5, 1.5)	Calibrated
Uncertainty multiplier for school contacts (m_S) [C]	Uniform (0.8, 1.2)	Calibrated
Prop. students on-site during "Partially open" periods [C]	Uniform (0.1, 0.5)	Calibrated
VE against infection	0.7	[1, 18, 8, 2, 10]
VE against hospitalisation	0.9	[3, 2, 10]
VE against death	0.9	[3, 10]
Time from symptom onset to hospitalisation (days)	Gamma (shape=5, mean=3)	[6]
Hospital stay duration (days)	Gamma (shape=5, mean=9)	[6]
Time from symptom onset to death (days)	Gamma (shape=10, mean=15.93)	[11]
Strain-specific parameters		
Wild-type strain		
Mean incubation period (days)	6.65	[24]
Delta variant		
Mean incubation period (days)	4.41	[24]
Relative intrinsic transmissibility (ref. wild-type)	1.5	[13, 15]
Relative risk of hospitalisation (ref. wild-type)	2.0	[4]
Relative risk of death (ref. wild-type)	2.3	[4]
Prop. escaping vaccine immunity against infection	0.3	[9, 14]
Omicron variant		
Mean incubation period (days)	3.42	[24]
Relative intrinsic transmissibility (ref. wild-type)	2.0	[9, 14]
Relative risk of hospitalisation (ref. wild-type)	0.82	[4, 16]
Relative risk of death (ref. wild-type)	0.71	[4, 16]
Prop. escaping vaccine immunity against infection	0.6	[9, 14]

Table S3: Age-specific parameters for wild-type COVID-19

Age group	Rel. suscepitbility to infection (ref. 15-69 y.o.) [25]	Proportion symptomatic [20]	Proportion of symptomatic patients hospitalised [19]	Infection fatality rate [17]
0-4	0.36	0.533	0.0777	0.00003
5-9	0.36	0.533	0.0069	0.00001
10-14	0.36	0.533	0.0034	0.00001
15-19	1.00	0.533	0.0051	0.00003
20-24	1.00	0.679	0.0068	0.00006
25-29	1.00	0.679	0.0080	0.00013
30-34	1.00	0.679	0.0124	0.00024
35-39	1.00	0.679	0.0129	0.00040
40-44	1.00	0.679	0.0190	0.00075
45-49	1.00	0.679	0.0331	0.00121
50-54	1.00	0.679	0.0383	0.00207
55-59	1.00	0.679	0.0579	0.00323
60-64	1.00	0.803	0.0617	0.00456
65-69	1.00	0.803	0.1030	0.01075
70-74	1.41	0.803	0.1072	0.01674
75-79	1.41	0.803	0.0703	0.03203
80 and above	1.41	0.803	0.0703	0.08292

vaccination- and strain-specific risks of hospitalisation and deaths, as well as statistical distributions of time to events to compute COVID-19-related hospital pressure and deaths over time.

1.3.1 COVID-19-related hospital pressure

The risk of hospitalisation given infection was expected to vary markedly by setting. For example, different countries may have different criteria for whether or not a COVID-19 patient should be admitted to a hospital. This makes it difficult to provide accurate estimates of hospitalisation rates for multiple countries.

For this reason we introduced a universal indicator named "hospital pressure" in our analysis. This indicator was obtained by considering the age-specific risk of hospitalisation given infection observed in the first year of the pandemic in the Netherlands, adjusted for vaccination status and for the infecting strain (Table S2). The "hospital pressure" indicator can therefore be interpreted as the level of hospital occupancy that would be observed in the analysed country if the rates of hospitalisation given infection in this country were the same as for the Netherlands. This quantity is expected to vary proportionately with occupancy over time, providing an indicator of hospital pressure. Note that this indicator was used in order to make comparisons between scenarios, such that one should interpret the relative differences between scenarios rather than the absolute values of the indicator.

Let us denote $i_{a,v,s}(t)$ the number of new disease episodes estimated to start at time t for people aged a with vaccination status v and infected with strain s. The number of new hospital admissions occurring at time t was calculated using the following convolution product:

$$\eta(t) = \sum_{a,v,s} \kappa_{a,v,s} \int_{u \geq 0} i_{a,v,s}(t-u) g_h(u) du \quad , \tag{7}$$

where $\kappa_{a,v,s}$ is the risk of hospitalisation given infection for age a, vaccination status v and strain s based on the Netherlands data, and g_h is the probability density function of the statistical distribution chosen to represent the time from symptom onset to hospitalisation (Table S2).

We then computed the "hospital pressure" quantity h, which is an indicator of hospital occupancy level, by combining the number of new hospital admissions η with the statistical distribution used to model hospital stay duration:

$$h(t) = \int_{u \geq 0} \eta(t-u)(1-\tau(u))du \quad , \tag{8}$$

where τ is the cumulative density function of the statistical distribution chosen to represent the hospital stay duration (Table S2).

1.3.2 COVID-19 deaths

We estimated the number of COVID-19 deaths over time using a similar approach as for the hospital pressure indicator. We used the age-specific infection fatality rates reported in O'Driscoll et al. [17], adjusted for vaccination status and for the infecting strain to estimate COVID-19 mortality. Using the same notations as in Section 1.3.1, the number of COVID-19 deaths observed at time t was obtained by:

$$\mu(t) = m_C \sum_{a,v,s} ifr_{a,v,s} \int_{u \geq 0} i_{a,v,s}(t-u) g_d(u) du \quad , \tag{9}$$

where $ifr_{a,v,s}$ is the risk of death given infection for age a, vaccination status v and strain s, and g_d is the probability density function of the statistical distribution chosen to represent the time from symptom onset to death (Table S2). We used the country-specific adjuster m_C to capture the fact that the infection fatality ratio is expected to vary by country, in part due to differences in COVID-19 death definition and reporting standards. This adjustment was automatically calibrated by the MCMC (Section 3).

2 Software and code used to conduct the analyses

2.1 Code

The Python code and data used to perform the analyses is fully available on Github at the following link: https://github.com/monash-emu/AuTuMN. In particular, the code associated with the implementation of the model is available here. The suite of functions used to run the model, perform calibration and analyse the outputs is available here. Finally, the model can be run for the included countries via an online Google Colab notebook, allowing the user to conduct their own analyses without any local software installation requirement. NEED TO CREATE NOTEBOOK

2.2 Software implementation

We used the *summer2* Python package (v 1.2.5) to implement the model. This is a domain specific library for compartmental epidemiological models that addresses a few of the key concerns as follows.

2.2.1 Application Programming Interface (API)

The model specification was done via a simple yet expressive Python API, while the numerical implementation was largely autogenerated by the *summer2* package at runtime. This specification is composable via stratification classes and other reusable components, thus the complexity of the software is kept to a minimum, reducing cognitive overhead and greatly reducing the possibility for error.

2.2.2 Optimising compiler

The *summer2* package uses the jax library as its computational backend, meaning that while the specification of models is done largely in Python, the model execution itself is transformed via an optimising compiler into fast native code. This brings the model runtime from several seconds (for a naive implementation) to under 50ms per iteration, which was necessary to perform the computationally-intensive calibration tasks described in Section 3.

3 Model calibration and uncertainty propagation

The model was calibrated using a Bayesian approach. In particular, we used the Adaptive Differential Evolution Metropolis (DEMetropolisZ) algorithm implemented with the *PyMC* Python package (v.5.2.0) to sample parameters from their posterior distributions. For each country, we ran 8 independent DEMetropolisZ chains of 35,000 iterations, each starting from a different starting point and using the first 5,000 draws for algorithm tuning. To determine the 8 starting points of the DEMetropolisZ chains, we conducted 8 independent optimisation searches using the Covariance Matrix Adaptation Evolution Strategy (CMA-ES) method, implemented with the *nevergrad* Python package (v.0.6.0) and with a budget of 10,000 model evaluations per search. The 8 optimisation searches' initial points were randomly drawn from Latin Hypercube Sampling (LHS) based on the parameter priors shown in Table S2. The parameters sampled with LHS were the transmission probability per contact, the IFR multiplier, the uncertainty multiplier for school contacts, and the proportion of students on-site during "Partially open" periods. The random process variables $W(t)$ (Section 1.2.6) were all set to 0 for each optimisation starting point.

Our calibration approach required a total of 360,000 ($8 \times (10000 + 35000)$) model evaluations per country analysis, which were completed in about two hours on a machine with 8 cpus and 32-GiB memory.

For each country, the results presented in the manuscript are associated with 1000 parameter sets randomly sampled from the posterior distributions obtained from DEMetropolisZ sampling (after discarding the first 25,000 iterations for each chain). The definitions of the prior distributions and the likelihood are detailed in the following sections.

3.1 Parameters varied during calibration

The parameters varied during calibration along with their associated prior distributions are listed in Table S2 and indicated with the superscript ^{C}. We used uniform prior distributions for all calibrated parameters. The primary parameters varied during calibration are the unadjusted risk of transmission per contact (β), the IFR multiplier (m_C), the original infection seeding time, the proportion of students on-site during "Partially open" periods, and the uncertainty multiplier modifying the school contacts' contribution (m_S).

Note that the values of the random process W_t described in Section 1.2.6 are also treated as calibrated parameters by the MCMC. The Gaussian auto-regressive component described in Equation 4 is incorporated in the posterior likelihood computation (Section 3.3).

3.2 Calibration targets

Model calibration was performed independently for each country. All models were fitted to the reported number of COVID-19 deaths over time. We used the daily number of COVID-19 deaths reported by WHO and applied a 7-day moving average to the observed data.

In addition, for countries where a nationally representative seroprevalence survey had been conducted (n=44), we include seroprevalence data in the calibration likelihood. We used the online platform SeroTracker to extract country-specific seroprevalence estimates. The estimates had to verify the following conditions to be included in the analysis as calibration targets:

- Be aligned with the World Health Organization's Unity protocol (WHO Unity) for general population seroepidemiological studies.
- Have a sample size greater than 599 (minimum sample size recommended in WHO sero-surveys protocol)
- Have a sampling start date later than 1 May 2020 (to avoid very early surveys that may be less accurate)
- Be nationally representative (as classified by SeroTracker)

We further excluded studies that focused on specific population subgroups presenting a risk of selection bias for seroprevalence (e.g. pregnant women, slum population, healthcare workers, quarantine workers).

Finally, to minimise the risk of interference with vaccination, we only included studies for which the vaccination coverage at the time of the survey (midpoint date) was lower than 10% of the measured seroprevalence.

All the criteria listed above were first verified systematically using the SeroTracker database, and the extracted studies were then analysed individually by one author (RR) to check that all inclusion criteria were verified.

When a seroprevalence study was restricted to a specific age-group, we matched the survey estimate to the modelled seroprevalence measured in the closest modelled age-group. For example, as the age-group reported in the Kenya survey was 16-64 years old, we used the modelled seroprevalence in the age-group 15-69 years-old to inform model calibration.

When multiple estimates were available for a country, we selected the highest ranked estimate after ordering by the following preference criteria (applied in the presented order):

1. Lowest risk of bias (according to SeroTracker),
2. Latest sampling start date (when a greater number of infections have occurred, and to avoid bias due to early geographic heterogeneity),

The estimates used to inform the models are summarised in Table S4, with the associated original reports accessible by clicking on the countries' names.

3.3 Likelihood definition

Let d_w denote the rounded average daily number of COVID-19 deaths during week w, and $\hat{d_w}^{\theta}$ the associated predicted number of deaths according to the model with parameter set θ.

For countries with seroprevalence data, let us denote π the measured seroprevalence proportion extracted from SeroTracker (Section 3.2). Let $\hat{\pi}^{\theta}$ denote the modelled age-matched proportion ever infected by the time the survey was conducted (using the midpoint date) associated with the parameter set θ. The likelihood was defined as follows for countries with seroprevalence data:

$$\mathcal{L}(\theta) := f_{\sigma}(\pi|\hat{\pi}^{\theta}) \times \prod_{w} g_r(d_w|\, \hat{d_w}^{\theta}) \quad , \tag{10}$$

where $f_{\sigma}(.|\mu)$ is the probability density function of a $[0,1]$-truncated normal distribution with mean μ and standard deviation σ; and $g_r(.|\mu)$ is the probability mass function of a negative binomial distribution with mean μ and overdispersion parameter r. The overdispersion parameter r was automatically estimated by the MCMC algorithm, while the standard deviation σ was set to different values depending on the SeroTracker-reported risk of bias associated with the seroprevalence estimate ($\sigma = 0.05$ if "Low", $\sigma = 0.1$ if "Moderate", $\sigma = 0.2$ if "High").

For countries without seroprevalence data, the likelihood equation reduces to:

$$\mathcal{L}(\theta) := \prod_{w} g_r(d_w|\, \hat{d_w}^{\theta}) \quad . \tag{11}$$

The likelihood functions described above represent the goodness of fit of a particular model parameterisation with regards to the targeted data. This quantity needs to be adjusted for the prior likelihood of the parameter set in order to compute the MCMC acceptance quantity $\mathcal{Q}(\theta)$. As we used uniform priors for all the parameters, the inclusion of the individual parameters' priors in the acceptance quantity is not necessary. Indeed, their respective contributions would cancel out as the same quantity would appear in the numerator and the denominator of the MCMC acceptance quantity ratio. However, the auto-regressive relationship described in Equation 4 must be accounted for as part of the combined prior likelihood of a parameter set. This prevents unrealistically large fluctuations of the random process. If W^{θ} represents the random process associated with the parameter set θ, the overall MCMC acceptance quantity is obtained by:

$$\mathcal{Q}(\theta) = \mathcal{L}(\theta) \times \prod_{i=1}^{n} z_{W_{i-1}^{\theta},\epsilon}(W_i^{\theta}) \quad , \tag{12}$$

where $z_{\mu,\epsilon}(.)$ represents the probability density function of the normal distribution $\mathcal{N}(\mu, \epsilon)$, and n is the number of random process updates.

Table S4: Seroprevalence data extracted from SeroTracker (national surveys).

country	sampling start date	sampling end date	age min	age max	denom. value	serum pos prevalence	estimate grade	overall risk of bias
Australia	2020-11-03	2021-03-12		19	1685	0.0023	National	High
Austria	2020-06-05	2020-12-04	18	72	20228	0.025	National	High
Belgium	2020-10-12	2020-10-17		101	2966	0.0418	National	Low
Brazil	2020-05-14	2020-06-23			89362	0.023	National	Moderate
Canada	2021-04-13	2021-04-30	17		16931	0.2692	National	Moderate
Chile	2020-09-25	2020-11-25	7	94	2493	0.104	National	Low
Colombia	2020-09-21	2020-12-11	5	80	17863	0.3253	National	Moderate
Croatia	2020-12-15	2021-02-15			1436	0.251	National	High
Czechia	2021-02-01	2021-03-31	18		19548	0.51	National	High
Denmark	2020-12-01	2020-12-31	12		4044	0.043	National	Low
Ecuador	2020-10-12	2020-10-19			1250	0.1168	National	Moderate
Egypt	2021-01-15	2021-06-15			2360	0.463	National	Moderate
France	2020-05-11	2020-05-17			3592	0.0493	National	Low
Germany	2020-10-26	2020-11-18	18		9929	0.011	National	Moderate
Honduras	2020-06-16	2020-06-23	5		792	0.062	National	Moderate
Hungary	2020-05-01	2020-05-16	14		10474	0.0068	National	Low
India	2020-12-18	2021-01-06	10		28598	0.241	National	Low
Iran	2021-01-15	2021-03-15	10	90	7411	0.342	National	Low
Israel	2020-06-28	2020-09-14			54357	0.046	National	Moderate
Italy	2020-05-25	2020-07-15			64660	0.025	National	Moderate
Japan	2020-06-01	2020-06-07	20		7950	0.001	National	Moderate
Jordan	2020-12-27	2021-01-06			5044	0.342	National	Moderate
Kazakhstan	2020-07-16	2021-07-07			85346	0.63	National	High
Kenya	2021-01-03	2021-03-15	16	64	3018	0.485	National	Moderate
Lebanon	2020-12-07	2021-01-15			2058	0.185	National	Low
Lithuania	2020-08-10	2020-09-10	18	92	3089	0.014	National	Moderate
Malawi	2020-10-14	2020-12-08			4261	0.078	National	Low
Mexico	2020-08-15	2020-11-15	3	12	944	0.187	National	Low
Nepal	2020-10-09	2020-10-22			3040	0.144	National	Low
Nigeria	2021-06-29	2021-08-21			4904	0.789	National	Moderate
Norway	2020-12-27	2021-02-13			1912	0.032	National	Moderate
Oman	2020-11-08	2020-11-19	5		4064	0.22	National	Moderate
Pakistan	2020-10-21	2020-11-08			4998	0.0702	National	Moderate
Portugal	2020-09-08	2020-10-14			13398	0.022	National	Moderate
Senegal	2020-06-15	2020-10-15			3231	0.204	National	High
Singapore	2020-11-15	2020-12-15	23	83	937	0.0016	National	High
Slovenia	2020-10-17	2020-11-10		99	1211	0.0429	National	Low
South Africa	2021-01-15	2021-05-15	15	69	16762	0.474	National	Moderate
Rep. of Korea	2020-09-24	2020-12-09	18	86	4085	0.0039	National	Moderate
Spain	2020-06-08	2020-06-22			62167	0.052	National	Low
Sweden	2020-11-23	2020-12-04			3183	0.07	National	Moderate
USA	2020-08-09	2020-12-08	18		4654	0.0471	National	Low
UK	2020-08-24	2020-09-18	17		8230	0.061	National	Low
Zambia	2020-07-04	2020-07-27			2704	0.021	National	Low

References

[1] Tiffany Charmet et al. “Impact of original, B.1.1.7, and B.1.351/P.1 SARS-CoV-2 lineages on vaccine effectiveness of two doses of COVID-19 mRNA vaccines: Results from a nationwide case-

control study in France". In: *The Lancet Regional Health – Europe* 8 (2021). DOI: 10.1016/j.lanepe.2021.100171. URL: https://doi.org/10.1016/j.lanepe.2021.100171.

[2] Noa Dagan et al. "BNT162b2 mRNA Covid-19 Vaccine in a Nationwide Mass Vaccination Setting". In: *New England Journal of Medicine* 384.15 (2021), pp. 1412–1423. DOI: 10.1056/NEJMoa2101765. URL: https://doi.org/10.1056/NEJMoa2101765.

[3] Public Health England. *COVID-19 vaccine surveillance report - Week 26*. Report. Jan. 2021. URL: https://www.gov.uk/government/publications/covid-19-vaccine-surveillance-report.

[4] David N. Fisman and Ashleigh R. Tuite. "Evaluation of the relative virulence of novel SARS-CoV-2 variants: a retrospective cohort study in Ontario, Canada". In: *Canadian Medical Association Journal* 193.42 (2021), E1619. DOI: 10.1503/cmaj.211248. URL: http://www.cmaj.ca/content/193/42/E1619.abstract.

[5] GISAID. *GISAID database*. Web Page. 2023. URL: https://gisaid.org/.

[6] Isaric Clinical Characterisation Group et al. "ISARIC COVID-19 Clinical Data Report issued: 27 March 2022". In: *medRxiv* (2022), p. 2020.07.17.20155218. DOI: 10.1101/2020.07.17.20155218. URL: http://medrxiv.org/content/early/2022/04/13/2020.07.17.20155218.abstract.

[7] Seran Hakki et al. "Onset and window of SARS-CoV-2 infectiousness and temporal correlation with symptom onset: a prospective, longitudinal, community cohort study". In: *The Lancet Respiratory Medicine* 10.11 (2022), pp. 1061–1073. DOI: 10.1016/S2213-2600(22)00226-0. URL: https://doi.org/10.1016/S2213-2600(22)00226-0.

[8] Victoria Jane Hall et al. "COVID-19 vaccine coverage in health-care workers in England and effectiveness of BNT162b2 mRNA vaccine against infection (SIREN): a prospective, multicentre, cohort study". In: *The Lancet* 397.10286 (2021), pp. 1725–1735. DOI: 10.1016/S0140-6736(21)00790-X. URL: https://doi.org/10.1016/S0140-6736(21)00790-X.

[9] Neda Jalali et al. "Increased household transmission and immune escape of the SARS-CoV-2 Omicron compared to Delta variants". In: *Nature Communications* 13.1 (2022), p. 5706. DOI: 10.1038/s41467-022-33233-9. URL: https://doi.org/10.1038/s41467-022-33233-9.

[10] Alejandro Jara et al. "Effectiveness of an Inactivated SARS-CoV-2 Vaccine in Chile". In: *New England Journal of Medicine* 385.10 (2021), pp. 875–884. DOI: 10.1056/NEJMoa2107715. URL: https://doi.org/10.1056/NEJMoa2107715.

[11] Malahat Khalili et al. "Epidemiological characteristics of COVID-19: a systematic review and meta-analysis". In: *Epidemiology and Infection* 148 (2020), e130. DOI: 10.1017/S0950268820001430. URL: https://www.cambridge.org/core/article/epidemiological-characteristics-of-covid19-a-systematic-review-and-metaanalysis/8B565B2FE5A97054E8B2564FB2CE6D3E.

[12] Ben Killingley et al. "Safety, tolerability and viral kinetics during SARS-CoV-2 human challenge in young adults". In: *Nature Medicine* 28.5 (2022), pp. 1031–1041. DOI: 10.1038/s41591-022-01780-9. URL: https://doi.org/10.1038/s41591-022-01780-9.

[13] Q. Li et al. "Early Transmission Dynamics in Wuhan, China, of Novel Coronavirus-Infected Pneumonia". In: *N Engl J Med* 382.13 (2020), pp. 1199–1207. DOI: 10.1056/NEJMoa2001316. URL: https://www.ncbi.nlm.nih.gov/pubmed/31995857.

[14] Frederik Plesner Lyngse et al. "Household transmission of the SARS-CoV-2 Omicron variant in Denmark". In: *Nature Communications* 13.1 (2022), p. 5573. DOI: 10.1038/s41467-022-33328-3. URL: https://doi.org/10.1038/s41467-022-33328-3.

[15] Zhang Meng et al. "Transmission Dynamics of an Outbreak of the COVID-19 Delta Variant B.1.617.2 — Guangdong Province, China, May–June 2021". In: *China CDC Weekly* 3.27 (2021), pp. 584–586. DOI: 10.46234/ccdcw2021.148. URL: https://weekly.chinacdc.cn//article/id/eb772589-1584-4ef9-beac-cac3ab2fbb12.

[16] T. Nyberg et al. "Comparative analysis of the risks of hospitalisation and death associated with SARS-CoV-2 omicron (B.1.1.529) and delta (B.1.617.2) variants in England: a cohort study". In: *Lancet* 399.10332 (2022), pp. 1303–1312. DOI: 10.1016/s0140-6736(22)00462-7.

[17] M. O'Driscoll et al. "Age-specific mortality and immunity patterns of SARS-CoV-2". In: *Nature* 590.7844 (2021), pp. 140–145. DOI: 10.1038/s41586-020-2918-0. URL: https://www.ncbi.nlm.nih.gov/pubmed/33137809.

[18] Emma Pritchard et al. “Impact of vaccination on new SARS-CoV-2 infections in the United Kingdom”. In: *Nature Medicine* 27.8 (2021), pp. 1370–1378. DOI: 10.1038/s41591-021-01410-w. URL: https://doi.org/10.1038/s41591-021-01410-w.

[19] Netherlands RIVM. *Epidemiologische situatie COVID-19 in Nederland*. Government Document. 2020. URL: https://www.rivm.nl/sites/default/files/2020-08/COVID-19_WebSite_rapport_wekelijks_20200804_1306.pdf.

[20] Pratha Sah et al. “Asymptomatic SARS-CoV-2 infection: A systematic review and meta-analysis”. In: *Proceedings of the National Academy of Sciences* 118.34 (2021), e2109229118. DOI: 10.1073/pnas.2109229118. URL: http://www.pnas.org/content/118/34/e2109229118.abstract.

[21] Anika Singanayagam et al. “Duration of infectiousness and correlation with RT-PCR cycle threshold values in cases of COVID-19, England, January to May 2020”. In: *Eurosurveillance* 25.32 (2020), p. 2001483. DOI: doi:https://doi.org/10.2807/1560-7917.ES.2020.25.32.2001483. URL: https://www.eurosurveillance.org/content/10.2807/1560-7917.ES.2020.25.32.2001483.

[22] Caroline Stein et al. “Past SARS-CoV-2 infection protection against re-infection: a systematic review and meta-analysis”. In: *The Lancet* 401.10379 (2023), pp. 833–842. DOI: 10.1016/S0140-6736(22)02465-5. URL: https://doi.org/10.1016/S0140-6736(22)02465-5.

[23] UNESCO. *UNESCO Global Monitoring of School Closures Caused by the COVID-19 Pandemic*. Web Page. 2023. URL: https://covid19.uis.unesco.org/global-monitoring-school-closures-covid19/.

[24] Yu Wu et al. “Incubation Period of COVID-19 Caused by Unique SARS-CoV-2 Strains: A Systematic Review and Meta-analysis”. In: *JAMA Network Open* 5.8 (2022), e2228008–e2228008. DOI: 10.1001/jamanetworkopen.2022.28008. URL: https://doi.org/10.1001/jamanetworkopen.2022.28008.

[25] J. Zhang et al. “Changes in contact patterns shape the dynamics of the COVID-19 outbreak in China”. In: *Science* 368.6498 (2020), pp. 1481–1486. DOI: 10.1126/science.abb8001. URL: https://www.ncbi.nlm.nih.gov/pubmed/32350060.

Figure S4: Modelled vaccine coverage (lines) against data (dots).

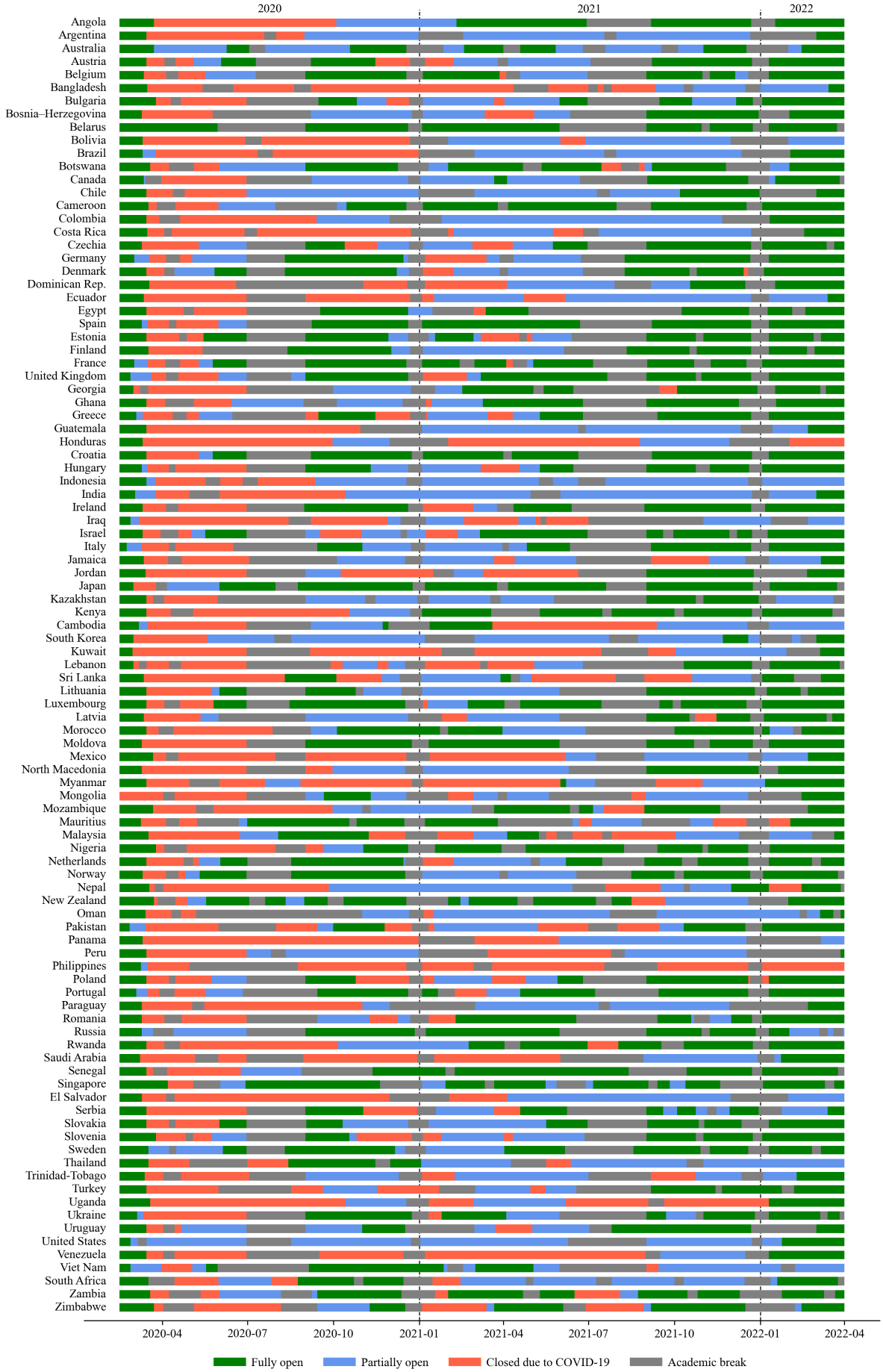

Figure S5: UNESCO data on school closures during the COVID-19 pandemic.

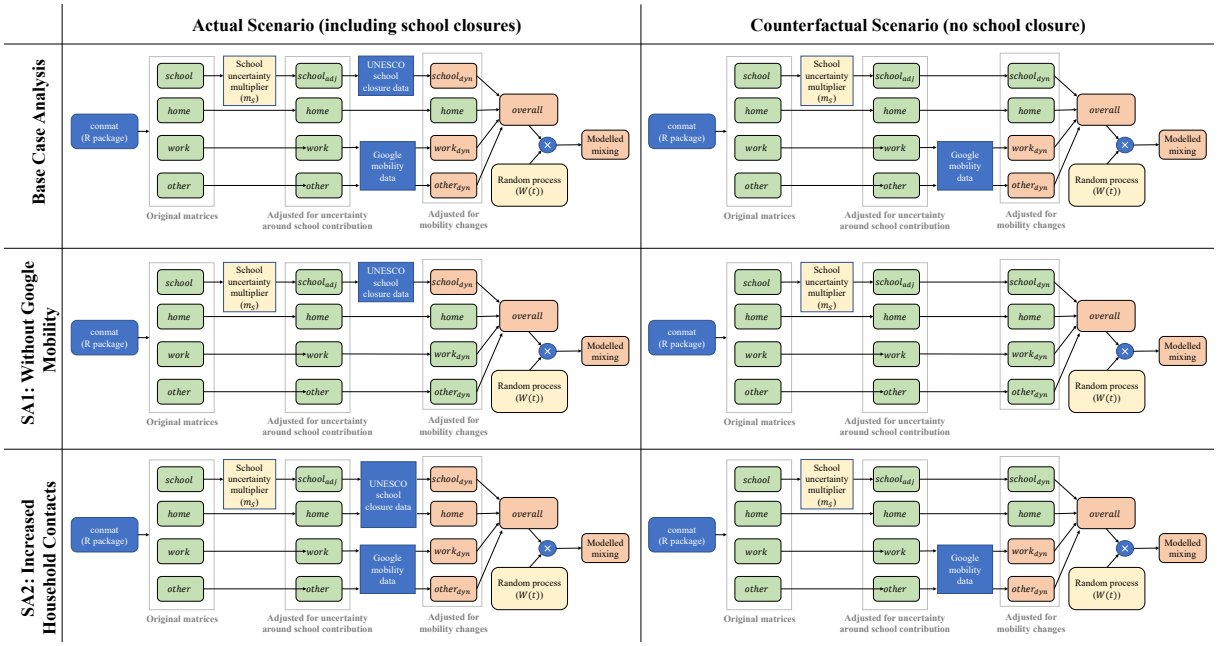

Figure S6: Modelled social mixing under Base Case and Sensitivity Analyses.